Structure-dependent adsorption and desorption of hydrogen on FCC and HCP cobalt surfaces

C.J. (Kees-Jan) Weststrate[a*], Daniel Garcia Rodriguez[b], Devyani Sharma[b], J.W. (Hans) Niemantsverdriet[a,c]

[a]SynCat@DIFFER, Syngaschem BV, P.O. Box 6336, 5600 HH Eindhoven, The Netherlands

[b] Dutch Institute for Fundamental Energy Research (DIFFER), Eindhoven, The Netherlands

[c]SynCat@Beijing, Synfuels China Technology Co. Ltd., Leyuan South Street II, No. 1, Huairou District, 101407 Beijing, China

*Corresponding author c.j.weststrate@syngaschem.com

***Abstract*:**

The interaction of hydrogen with cobalt surfaces is of fundamental interest for Fischer-Tropsch synthesis. In the present work, the adsorption and desorption of hydrogen was studied on various cobalt single crystal surfaces that together represent the surface structures exposed by FCC and HCP cobalt nanoparticles used in applied catalysis. Dissociative hydrogen adsorption is activated on flat Co(0001), especially for hydrogen coverages beyond 0.5 ML. A tungsten filament creates hot hydrogen molecules and hydrogen atoms that together increase the dissociative sticking probability and make it possible to obtain hydrogen coverages above 0.5 ML. Hydrogen in excess of 0.5 ML binds more weakly and desorbs in a separate low temperature desorption peak, in line with theoretical predictions. A third desorption peak appears above 1 ML and is attributed to subsurface hydrogen, the formation of which is attributed to hydrogen atoms produced by the tungsten filament. Adsorbed hydrogen atoms form (islands) of an ordered (2×2)- 2H honeycomb structure for coverages between 0.3-0.8 ML which points to a specific stability of this structure. Step and kink sites on vicinal close-packed surfaces provide a low energy path for both hydrogen adsorption *and* desorption which results in a much higher dissociative sticking probability and a lower desorption temperature.

The hydrogen adsorption strength on various FCC and HCP cobalt surfaces varies between 30 and 45 kJ/mol H_{ad} and is strongest on threefold hollow sites on the close-packed terraces while it is significantly lower on fourfold hollow sites on FCC-(100) and on threefold hollow sites on various open HCP surfaces. Under reaction conditions, the structure-dependent adsorption energy translates to a two to three orders of magnitude variation of the equilibrium constant for hydrogen.

Introduction

Fischer-Tropsch Synthesis (FTS) is a technologically important process in which synthesis gas, a mixture of H_2 and CO, is converted into long chain hydrocarbons. Both iron- and cobalt-based catalysts are used industrially for this process [1]. FTS is seen as a vital ingredient of future energy schemes for converting renewable electricity via electrolysis to H_2 and combining it with CO_2 to produce liquid hydrocarbon fuels [2]. Hydrogen atoms adsorbed on the surface of the catalyst participate in many of the elementary reaction steps that ultimately transform CO and H_2 into C_xH_y and H_2O. Despite the relevance of cobalt as a hydrogenation catalyst in synthesis gas reactions, the number of experimental studies about hydrogen adsorption on single crystal surfaces of cobalt is limited [3–10].

Several different well-defined single crystal surfaces of cobalt were used in the present work to investigate how the structure of the catalyst surface affects its interaction with hydrogen. The single crystals were chosen such that the most typical structural elements exposed on the surface of a cobalt nanoparticle are included, as illustrated in figure 1. Cobalt FTS catalysts contain nano-crystallites of a diameter smaller than 20 nm [1], for which the FCC bulk structure is thermodynamically preferred [11]. A Wulff construction of an FCC-Co particle indicates that close-packed (111) facets account for 70% of the surface while (100) is the second-most abundant surface and accounts for around 20% of the surface. Atomistic models of FCC-

particle shapes indicate that the remaining ~10% consists of undercoordinated atoms at steps and kink sites [12–14].

Cobalt single crystals can only be prepared in high quality with a HCP bulk structure, but the HCP-Co(0001) surface is structurally very similar to the FCC-(111) surface so that it can serve as a model system for 70% of the FCC particle surface that exposes this close-packed surface. The reactivity of steps and kinks was studied using Co(10-120), Co(10-19) and Co(11-29) surfaces. These are high Miller index HCP surfaces that expose monoatomic steps and kinks separated by close-packed terraces. The ABAB stacking of the close-packed layers in HCP cobalt causes the structure of the step edge sites on vicinal surfaces to alternate between A and B-type steps which makes it impossible to determine eventual reactivity differences between the two step types [15,16].

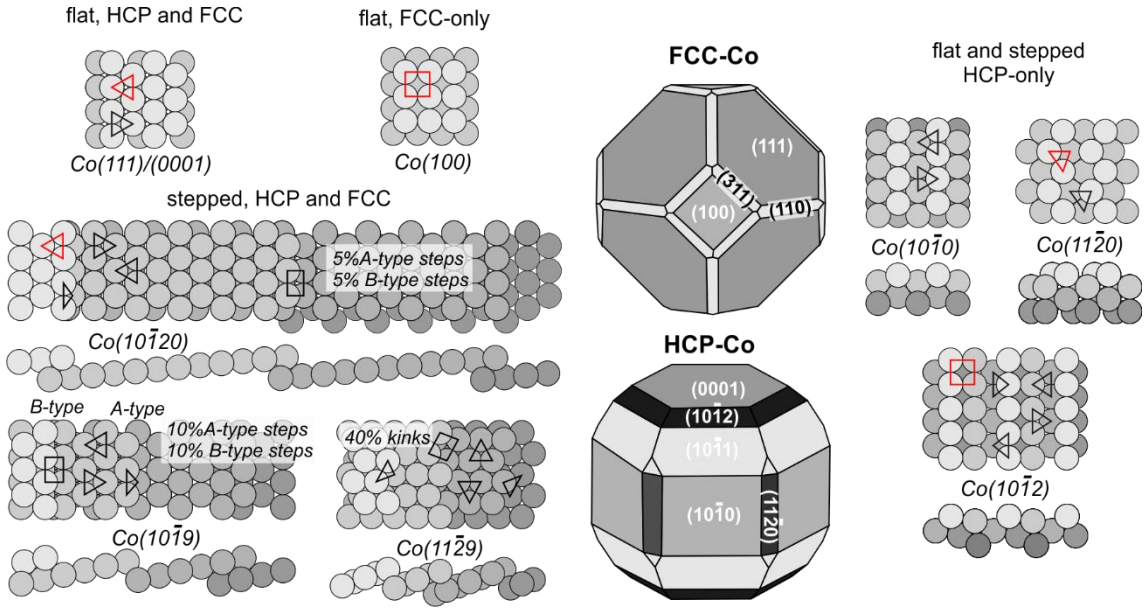

Fig. 1: *Surface structures of various Co single crystal surfaces studied in the present work together with Wulff construction of a HCP and FCC cobalt particle, respectively, indicating the location and abundance of the different facets (adapted from ref.* [17]*). Various possible adsorption sites for* H_{ad} *are indicated, where the most favourable sites predicted by DFT calculations in refs.* [4,7] *are marked in red.*

As there is no HCP surface that is structurally equivalent to FCC-Co(100), this surface cannot be studied using a cobalt single crystal. Consequently, thus far only theory calculations have been used to study the interaction of FCC-Co(100) with H_2 [4]. By using a Cu(100) substrate to grow an epitaxial layer of Co [18,19] we were able to study the interaction of H_2 with the FCC-Co(100) surface experimentally for the first time.

Studies by Kwak et. al. suggest that (metastable) HCP-Co nanoparticles show improved catalytic performance for FTS [20,21] compared to FCC-Co. The Wulff construction for HCP-cobalt particles predicts that the close-packed surface accounts for only 14-18% of the particle surface [13,22]. HCP-particles expose monoatomic step and kink sites similar as those on FCC-Co, but they also exhibit surface terminations that are unique for HCP particles, such as Co(10-10) [3], the second-most stable HCP-Co surface [17,22], Co(10-11), as well as other more open surfaces such as Co(11-20) and Co(10-12) [7]. Adsorption and desorption of hydrogen has previously been studied experimentally on a number of these surfaces [3,7]. We here include results from these studies in the discussion to thereby provide a comprehensive overview of the structure sensitivity of hydrogen adsorption on both FCC and HCP cobalt surfaces. The findings provide detailed fundamental insights into how surface structure, surface temperature and gas temperature affect the dissociative sticking probability of hydrogen on cobalt and show that the hydrogen adsorption energy varies significantly with surface structure.

Experimental procedures: The experiments were performed in a UHV system with a base pressure of ~3×10^{-10} mbar which is equipped with LEED/Auger optics, a sputter gun for sample cleaning, a dual beam electron beam evaporator and two quadrupole mass spectrometers (QMS). One mass spectrometer is positioned in the main chamber and probes the residual gas while a second mass spectrometer is in a separately pumped compartment. For desorption studies the sample is placed around 2 mm away from the 5 mm wide opening of the differentially pumped QMS housing. This geometry eliminates desorption from other parts of

the sample holder but quantitative evaluation may be affected in cases where desorption occurs preferentially in one direction with respect to the surface normal [23]. The mass spectrometer located in the main chamber was used whenever possible to make quantification more reliable.

The disc-shaped Co(0001), Co(11-29), Co(10-19) and Co(10-120) samples with a diameter of 8 mm and a thickness of 2 mm were cut and polished to within 0.1 degree of the desired orientation by Surface Preparation Laboratory (SPL). The samples were clamped between the two legs of a U-shaped tungsten wire in thermal contact with a liquid nitrogen reservoir, enabling a minimum temperature of around 95 K. Sample heating was achieved by passing a direct current through the support wire. Sample temperatures were measured by a K-type thermocouple spotwelded to the backside of the sample. The samples were cleaned by cycles of (1 kV) Ar^+ sputtering while held at 650 K followed by annealing in vacuum (5-10 min.) at the same temperature. The sputter-damaged Co(0001) was created by sputtering (1 kV Ar^+) for 5 min. at 350 K followed by a 5 min. anneal at 350 K. Sample cleanliness was checked by LEED and Auger spectroscopy, as well as by H_2 and CO desorption [4,24–26]. Stepped surfaces were found to be particularly sensitive to irreversibly adsorbed contaminations from the residual gas (C and O from CO and/or H_2O dissociation [27]) and a short sputter-anneal cycle was performed after recording a series of 2-3 hydrogen desorption experiments. Measurements were repeated several times to verify reproducibility.

A disc-shaped Cu(100) crystal with a diameter of 8 mm and a thickness of 2 mm (SPL) was used as substrate to grow an FCC-Co(100) film. The copper sample was mounted in the same way as the Co crystals, with the thermocouple fixated in a small hole in the side of the sample as spotwelding is not possible on copper. The Cu(100) sample was cleaned by repeated sputter-annealing samples (1 kV, sputter at RT, flash anneal to 1000 K) until Auger spectra indicated a clean sample and LEED showed a sharp diffraction pattern. Co was deposited using an e-beam evaporator while the sample was held at room temperature. The system pressure rose to

around 1×10^{-9} mbar during evaporation and the QMS indicated that this was mainly H_2. The thickness of the Co film varied between the different experiments but was always in the order of 7-18 ML as determined from the attenuation of the Cu_{LMM} Auger electrons. After cobalt deposition the sample was annealed for 5 minutes at 470 K to desorb CO and H_{ads} adsorbed during evaporation and to anneal the sample surface while avoiding excessively high temperatures which are known to cause Cu segregation to the Co surface [28]. CO desorption was used to verify that no significant Cu was present at the surface, as the CO desorption peak below 200 K due to CO bound to copper was completely absent [18]. The sample temperature was kept below 550 K in all desorption experiments to minimize Cu segregation. Moreover, the Co film was regularly sputtered off and a new Co film was deposited to ensure minimal influence of Cu segregation and other contaminants. A Cu(111) sample which was used for reference measurements was mounted in the same manner as Cu(100) and the same cleaning procedure was used.

Hydrogen and deuterium were led through a cold trap held at liquid nitrogen temperature prior to introduction into the vacuum chamber. The absence of significant H_2O desorption (not shown here) even after H_2 doses in the order of kL, confirms that the trap effectively eliminated water from the gas. Doses are reported in Langmuir (1 L = 1×10^{-6} Torr·s) and were calculated using an ion gauge sensitivity factor of 0.46. Previous studies showed that dosing of H_2 on flat Co(0001) produces 0.5 ML as a maximum coverage [4,5,24,29] and this was used as a reference for quantification of the H_2 desorption spectra from Co(0001). The sample holder accommodates two crystals at the same time and the high Miller index cobalt crystals were mounted back-to-back with the Co(0001) crystal so that the desorption spectrum of 0.5 ML H_{ad} on the close-packed surface could be used as a quantitative reference to determine the hydrogen coverage on the vicinal Co surfaces [7,30].

The hot H_2 source consists of a tungsten coil with a wire diameter of 0.38 mm and a total length of about 12 cm. It was operated at 5-5.5 A, which resulted in a filament temperature between 1570-1640 K, as determined using a pyrometer. The filament was attached to a z-translator and was placed at ~10-30 mm away from the sample surface during dosing [see inset figure 2(a)]. The close proximity of the hot filament caused the sample temperature to slowly rise during dosing, and the filament-sample distance was adjusted so that the crystal stayed below 150 K during exposure to hydrogen. The filament was degassed prior to use and the background pressure in the system during operation of the filament remained at 3×10^{-10} mbar.

Results and discussion

H_2 adsorption and desorption on Co(0001) ≤1 ML

Previous studies show that the maximum H_{ad} coverage on Co(0001) that can be reached in a typical UHV experiment is only 0.5 ML [4,5,7,24]. Dosing H_2 with a hot tungsten filament (~1600 K) placed close to the sample surface [see inset of fig. 2(a)] makes it possible to reach higher coverages. Figure 2 shows a series of hydrogen desorption spectra obtained after dosing with hot filament on. For H_2 doses below 2 Langmuir (L) with the filament on, the coverage stays below 0.5 ML and the desorption spectra in this coverage regime are identical to those obtained without filament. The single desorption peak with second order desorption characteristics in this coverage regime is labelled as the β_2 peak following the nomenclature used for Ni(111) [23,31]. Higher doses with the filament on lead to the appearance of a second desorption peak around 300 K, labelled β_1. The coverage appears to stabilize around 0.8 ML after dosing ~55 L, but an order-of-magnitude increase of the dose (≥300 L) caused a further increase of the coverage. Quantitative analysis after saturation of the β_1 and β_2 peaks yields a value of 1 ML. A third desorption peak appears around 250 K for very high doses with filament on. We

tentatively assign the α desorption peak to subsurface hydrogen and is discussed in more detail hereafter.

The dosage-coverage plots recorded with and without filament in fig. 2(b) show that the hot filament increases the initial dissociative sticking probability by a factor of six. The enhanced sticking probability after heating the gas is in line with theoretical findings [4,32,33] which predict a small barrier of around 8 kJ mol^{-1} for dissociative H_2 adsorption on clean Co(0001). The gas temperature in a typical UHV experiment is around 300 K while the sample temperature is typically kept below 150 K to ensure irreversible adsorption. Under these conditions even a small barrier significantly slows down dissociative hydrogen adsorption on Co(0001) [4,5,7,24]. Theory calculations also indicate that the activation barrier for dissociative adsorption increases significantly above 0.5 ML[4] and this then explains why a coverage beyond 0.5 ML is typically not reached in UHV experiments.

The hot filament creates hydrogen atoms and 'hot' H_2 molecules that can overcome the barrier for dissociative adsorption. Studies about atomic hydrogen production by tungsten filaments go back to the work of Langmuir[34], and several relevant studies are available in older literature. Based on previous findings by Hickmott[35], we explored the efficiency of hydrogen atom production for our filament, as discussed in detail in the supporting information. In summary, we find that atomic hydrogen can be produced with a filament temperature of only 1600 K, but in quantities that are at least three times too small to account for the six-fold enhancement of the initial sticking coefficient. We therefore suggest that the enhanced sticking must to a significant extent be attributed to 'hot' hydrogen molecules which have a gained energy by interacting with the hot filament surface[36]. The higher reactivity of such 'hot' hydrogen molecules on Co(0001) is confirmed by the work of Jiang et al.[32] who used theoretical modelling to investigate dissociative hydrogen adsorption on Co(0001). They concluded that the barrier for dissociation is reactant-like, and dissociation is strongly promoted by

translational energy while higher vibrational and rotational energies have a much smaller effect [37]. Filling of the surface beyond 0.8 ML required much higher H_2 doses with the filament on. We suggest that the low vacancy concentration at this point strongly inhibits dissociative adsorption of H_2 molecules, a process that which requires two adjacent vacant sites. Hydrogen atoms instead require only a single vacant site and we propose that the small quantity of H produced by the filament is responsible for filling the surface beyond 0.8 ML.

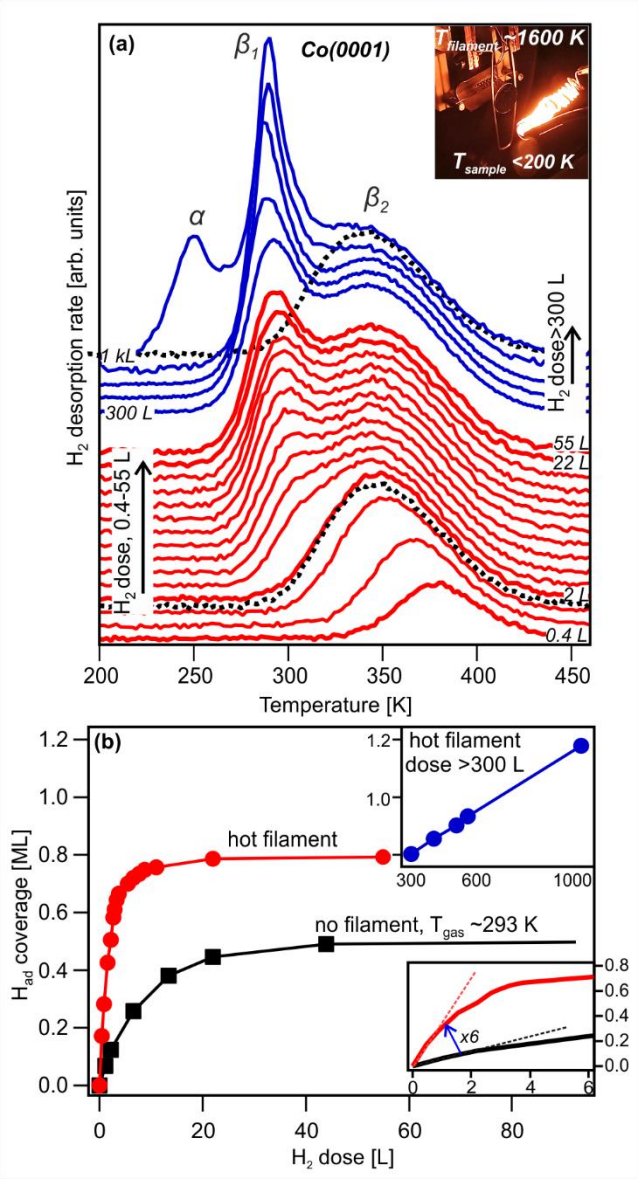

Fig. 2: *(a) H_2 desorption spectra after dosing H_2 <150 K with a hot filament (5 A, 1570 K) close to the surface (heating rate 2 Ks^{-1}). The black dashed line indicates the H_2 desorption*

spectrum corresponding to 0.5 ML, obtained after dosing 400 L without filament. (b) Hydrogen coverage as a function of H_2 dose, with (red filled circles) and without (black filled squares) hot filament. Populating the surface beyond 0.8 ML required significantly higher H_2 doses and these data are indicated in blue.

Chemisorbed hydrogen on Co(0001): adsorbate ordering

Hydrogen atoms adsorbed on Co(0001) form an ordered adsorbate layer for θ_H=0.5 ML which produces a (2×2) diffraction pattern in low energy electron diffraction (LEED) [24]. LEED was used after dosing hydrogen with the filament on to study ordering of the hydrogen atoms in the coverage regime above 0.5 ML. Figure 3 shows the diffraction patterns obtained during a stepwise heating sequence after adsorption of the equivalent of 1.2 ML atomic hydrogen.

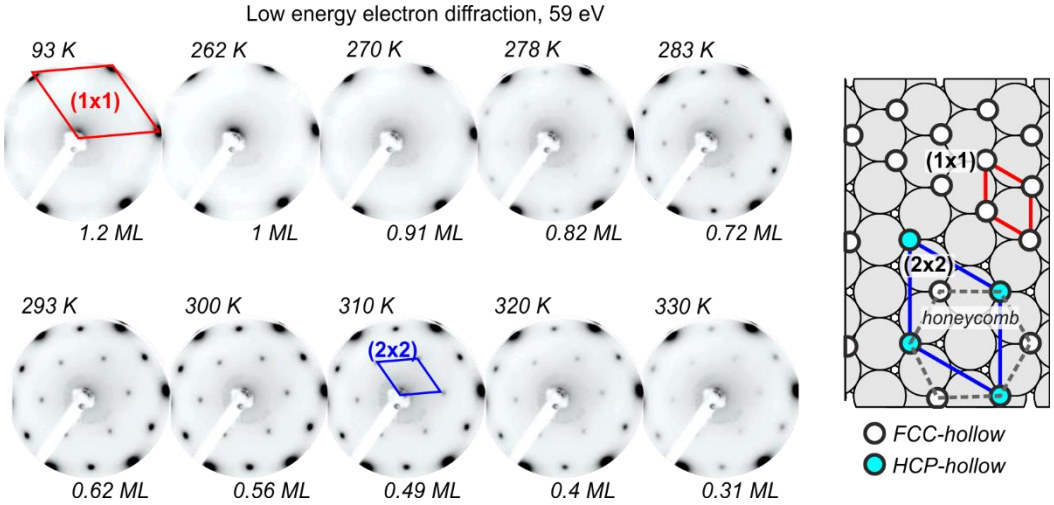

Fig. 3: *Low energy electron diffraction patterns at different hydrogen coverages on Co(0001), recorded below 120 K after stepwise heating to the indicated temperatures. The coverage after each heating step was determined from the m/z=2 (H_2) signal of the main chamber QMS. Structure models of the (1x1)-1H and (2x2)-2H honeycomb structure are shown on the right.*

The diffraction patterns above 0.9 ML only show the (1×1) diffraction spots of the Co(0001) substrate. The hydrogen most likely forms a (1×1) overlayer in this regime, as reported by Lewis et al. for hydrogen on close-packed Co nano-islands supported on Cu(111) [8]. A faint

(2×2) pattern becomes visible for $\theta_H \leq 0.8$ ML. The (2×2) diffraction spots increase in intensity and become sharper with decreasing hydrogen coverage, reaching a maximum intensity around 0.5 ML after which their intensity decreases again. We attribute the (2×2) pattern to a honeycomb structure with H atoms occupying equal amounts of FCC and HCP-hollow sites and with a total hydrogen coverage of 0.5 ML. This structure was experimentally observed on the close-packed cobalt nano-islands on Cu(111) by STM [8] and is also known to for Ni(111) [38].

The presence of a (2×2) diffraction pattern for H_{ad} coverages above 0.5 ML indicates the formation of islands with a local coverage of 0.5 ML surrounded by areas with a local higher coverage. For a hydrogen coverage below 0.5 ML the (2×2) islands must instead be surrounded by areas with a lower local hydrogen coverage. This points to a special stability of this structure that leads to inhomogeneities in the adsorbate layer. Lewis and co-workers used nanometer-sized close-packed cobalt islands on a Cu(111) substrate as a model system to study hydrogen adsorption by STM [8]. The undercoordinated atoms cobalt atoms at the edge of these bilayer cobalt islands promote dissociative H_2 adsorption so that hydrogen coverages beyond 0.5 ML can be obtained without a hot filament [4,7]. These authors also find the (2×2)-2H honeycomb structure for $\theta_H \leq 0.5$ ML and report an ordered (1×1) hydrogen overlayer at the saturation point. Mixtures of the two were found for intermediate coverages between 0.5-1 ML, in line with the LEED findings presented here. These authors also found a (3×3)-6H ($\theta_H = 2/3$) structure in this coverage regime alongside areas covered by either the (2×2)-2H or the (1×1)-1H structures. The diffraction experiments presented here do not show any diffraction spots that point to a (3×3) periodicity and we cannot confirm the existence of the (3×3)-6H structure on flat Co(0001).

Hydrogen adsorption on Co(0001): beyond 1 ML

The α desorption peak at 250 K was explored further by using doses in the kL (10^3 L) regime with the filament operated at a slightly higher temperature (5.5 A, 1640 K) compared to the series shown in Fig. 2.

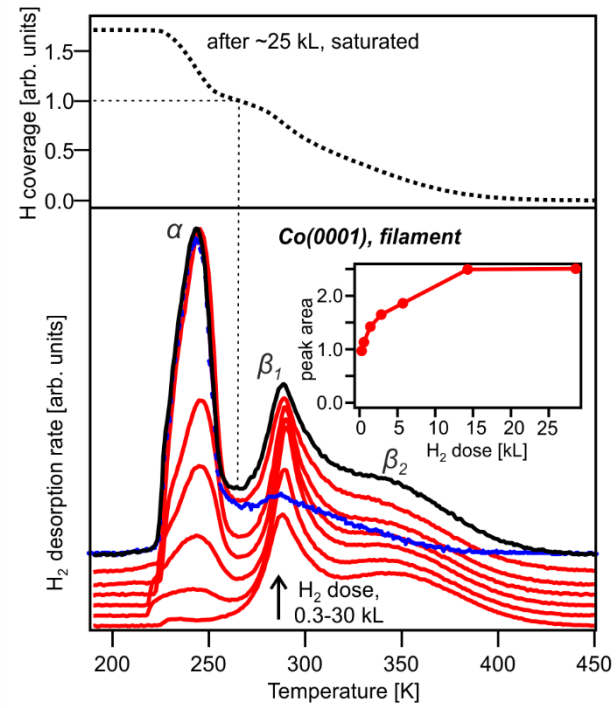

Fig. 4: *H_2 desorption spectra (2 Ks^{-1}) after prolonged exposure of the Co(0001) surface to H_2 (1 kL = 10^3 L) with the hot filament on (5.5 A, 1640 K). The inset shows the total peak area normalized to the first spectrum in the series. The upper panel shows the integral of the 25 kL spectrum where the sum of the β_1 and β_2 peak areas was assumed to be 1 ML. The spectrum in blue shows the difference between the first spectrum and the 'high dose' spectrum.*

Figure 4 shows the H_2 desorption spectra recorded after dosing large quantities of H_2 with the filament on. The desorption peak area stabilizes after dosing ~15 kL and quantitative analysis

of the peak area relative to the first spectrum in the series yields a hydrogen quantity equivalent to 2.5 ML. This is quite different from the value of 1.7 ML found when the integrated peak area of the 25 kL spectrum is normalized by assuming that the area of the β_1 and β_2 desorption peaks corresponds to 1 ML (see fig. 4, upper part). This discrepancy is also evident from the difference spectrum between the first and last spectrum of the series, shown in blue in fig. 4, which shows that the growth of the α peak is accompanied by an increase of the β_1 and β_2 peak intensity. These two peaks correspond to well-defined surface coverages of 1 and 0.5 ML, respectively, and it is unlikely that their growth corresponds to an increase of the hydrogen *surface* coverage. We instead attribute this peculiar behaviour to hydrogen located in sub-surface sites. On Ni(111) subsurface hydrogen was identified by electron energy loss spectroscopy [31] after dosing hydrogen atoms. Subsurface hydrogen in that case produces an additional H_2 desorption peak on the low temperature side of the β_1 and β_2 peaks, similar to the α peak found in the present work. On Ni(111) subsurface hydrogen could only be formed by dosing atomic hydrogen which is produced in small quantities by the filament. A recent study used an efficient hydrogen atom source [39] to dose hydrogen atoms onto a polycrystalline cobalt foil. It was found that exposure to hydrogen atoms produced an additional low temperature desorption peak which was attributed to subsurface hydrogen. Like in our case, the intensities of the β_1 and β_2 desorption peaks were found to increase along with the growth of the low temperature desorption peak attributed to atomic hydrogen. We tentatively suggest that the apparent growth of the β_1 and β_2 peaks is caused by a high temperature tailing of the subsurface desorption peak caused by the slow release of H atoms from subsurface layers that continues up to 350 K.

H_2 adsorption and desorption on FCC-Co(100)

Co deposited onto Cu(100) at RT forms a closed layer of low corrugation that follows the structure of the copper substrate [18,19], and this approach was used to study the interaction of H_2

with FCC-Co(100). The LEED pattern [see SI] shows sharp diffraction spots after evaporation and annealing, indicating that a flat FCC-Co(100) surface was obtained. Several checks were performed to verify that the findings on Co/Cu(100) are representative of FCC-Co(100). Experiments provided in the supporting information show that the hydrogen desorption peak shapes and temperatures from a 7 ML and a 18 ML cobalt film are very similar, a first indication that a 7 ML layer is already thick enough to eliminate the influence of the underlying copper substrate. Further confirmation comes from experiments in which ~11 ML Co was deposited onto a Cu(111) substrate. The H_2 and CO desorption spectra from the Co/Cu(111) system are very similar to those from Co(0001) [see SI], which confirms that the influence of the Cu substrate on the reactivity of cobalt overlayers appears to be negligible, provided these are thicker than about 7 layers.

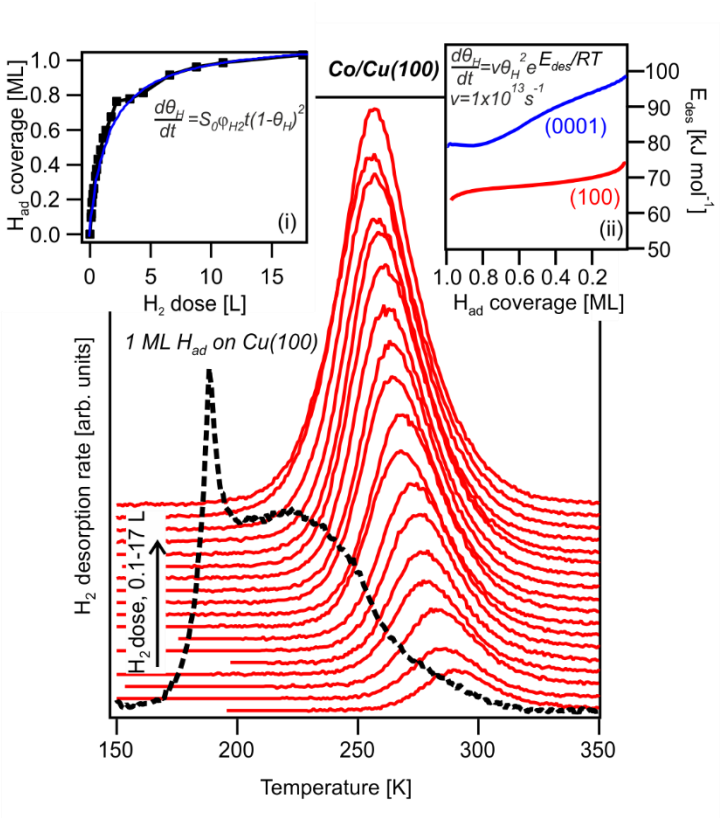

Fig. 5. *H_2 desorption from ~11 ML Co/Cu(100) after dosing at 100 K. The spectrum shown by a dashed black line corresponds to desorption of 1 ML H_{ad} from the Cu(100) and serves*

as a quantitative reference for H_2 desorption from Co/Cu(100). Inset (i) shows the dosage-coverage curve. Inset (ii) shows a comparison of the coverage-dependent activation energy of desorption for Co(0001) and FCC-Co(100). A heating rate of 2 Ks^{-1} was used.

Fig. 5 shows a series of H_2 desorption spectra for an 11 ML Co/Cu(100) sample. We note that a fresh Co layer was prepared after recording three desorption spectra to minimize the influence of contaminants and Cu segregation. Desorption of 1 ML H_{ad} from the clean Cu(100) substrate (created by dosing H_2 with the hot filament) was used as a reference [40] to normalize the desorption peak area and is provided in the figure. The coverage-dose plot [inset (i)] shows that the hydrogen coverage on Co(100) saturates at 1 ML, with an initial sticking coefficient that is around 20 times higher than on the flat, close-packed Co(0001) surface. The coverage-dosage curve can be described by $r_{ads}=S_0 \cdot \varphi_{H2} \cdot t \cdot (1-\theta_H)^2$, as shown in inset (i), where S_0 is the initial sticking probability, φ_{H2} the influx of hydrogen molecules and $(1-\theta_H)$ the concentration of free sites. The quadratic dependence on free site concentration causes a rapid drop of the adsorption rate as the coverage increases so that a rather high dose of 20 L of is to reach the saturation point of 1 ML.

Hydrogen desorption from Co(100) shows a single desorption peak for all coverages, with a peak maximum that shifts with increasing coverage as recombinative hydrogen desorption is a second-order process. The much narrower desorption peak shape compared to that of the β_2 peak on Co(0001) combined with the presence of only one instead of two desorption peaks for θ_H=1 ML indicates that the desorption barrier on FCC-Co(100) depends much less on the hydrogen coverage than on Co(0001). The different coverage dependence was explored further by calculating the coverage-dependent desorption barrier for both surfaces using a second-order Polanyi-Wigner rate expression and by assuming a constant pre-factor of 1×10^{13} s^{-1}. The resulting desorption barrier as a function of coverage, shown in inset (ii), is around 70 kJ mol^{-}

[1] for FCC-Co(100) and varies very little with hydrogen coverage. On Co(0001) the analysis yields a barrier of around 98 kJ mol^{-1}, but also shows a significant decrease as a function of coverage. These experimental findings show a qualitative match with the DFT calculations reported in refs. [4,7] which predict that the hydrogen adsorption energy a lower adsorption energy on FCC-Co(100) in the low coverage limit and show that it remains constant as the hydrogen coverage increases. On Co(0001) the adsorption energy the adsorption energy in the low coverage limit is higher, but it decreases with increasing surface coverage.

The supporting information provides a comparison of the experimental desorption spectra with the simulated desorption spectra shown in ref. [4] which are based on DFT calculations. For Co(0001) an excellent match is found between experiment and theory, both in terms of the desorption peak shape and the desorption temperature. For FCC-Co(100) the shape of the desorption peak is also modelled very well by the DFT data, but for this surface the desorption temperature in the model is significantly higher than in the experiment. This at first glance suggests that the DFT functional used in ref. [4] is more accurate for Co(0001) than for FCC-Co(100), but in reality the functional used somewhat overestimates the hydrogen adsorption energy for both surfaces. The *apparent* better match between experiment and theory on Co(0001) is attributed to an artefact of the simulations that stems from the assumption that the desorption barrier is equal to the computed adsorption energy. We hereafter show that hydrogen adsorption on Co(0001) is slightly activated while it is not activated on FCC-Co(100). The non-zero adsorption barrier on Co(0001) needs to be added to the adsorption energy to obtain an accurate desorption barrier. Adding a small adsorption barrier to the desorption barrier used in the simulations for Co(0001) would shift the simulated desorption spectra to higher temperature and create a mismatch between experiment and theory similar to the mismatch found for FCC-Co(100).

Activated vs unactivated adsorption: surface temperature dependence

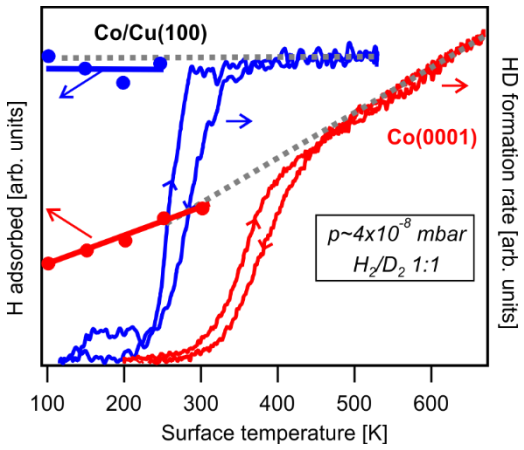

Fig. 6: *H_2 adsorption on Co(0001) and FCC-Co(100) as a function of surface temperature. The markers <300 K show the quantity of H adsorbed after dosing a constant amount of H_2 [0.11 L for Co(100), 2.2 L for Co(0001)] at different surface temperatures. The solid lines show HD (m/z=3) production during heating and cooling Co(0001) and FCC-Co/Cu(100) in a 1:1 mixture of H_2 and D_2 at a total pressure of ~4×10^{-8} mbar (1 Ks^{-1}). The HD production is directly proportional to the dissociative initial sticking coefficient as explained in the text. Note that the initial sticking probabilities of the two surfaces are very different and a different y-scaling was applied to each dataset to emphasize the different trend for the two surfaces.*

The surface temperature dependence of hydrogen adsorption on FCC-Co(100) and Co(0001) was studied to get more insight into the activation barrier for adsorption, as shown in figure 6. Below ~300 K the dependence of hydrogen adsorption on surface temperature was determined by dosing the same (small) amount of H_2 at different surface temperatures followed by TPD to measure θ_H. At higher surface temperatures the temperature-dependent hydrogen adsorption rate was determined by measuring the HD production rate during heating and cooling in presence of a 50/50 mixture of H_2/D_2 [41]. A dynamic adsorption-desorption equilibrium is established at high surface temperature and as the surface is covered with a mixture of adsorbed H_{ad} and D_{ad}, desorption produces HD (m/z=3) at a rate that is proportional to the total desorption rate. At equilibrium the desorption rate is equal to the adsorption rate so that r_{des}=

$r_{ads}= \varphi_{H2}(p,T_{gas})S_0(1-\theta_H)^2$, where φ is the impingement rate, S_0 the initial sticking probability, and $(1-\theta_H)$ the concentration of vacancies. The impingement rate remains constant throughout the experiment and since the steady state hydrogen concentration is very low the term $(1-\theta_H)$ drops out as well. The equation thus reduces to: $r_{HD} \propto S_0$, i.e. changes of the HD production rate as a function of surface temperature can be attributed to changes in the initial sticking probability. The combined findings at low and high temperature show that the initial dissociative sticking probability does not depend on surface temperature for FCC-Co(100) while it increases with surface temperature for Co(0001). This shows that hydrogen adsorption is activated on Co(0001) while it is not activated on Co(100) and explains the twenty times higher initial sticking probability found *at 100 K* for hydrogen on FCC-Co(100).

H_2 adsorption and desorption on Co(10-120), Co(10-19) and Co(11-29): the influence of steps and kinks

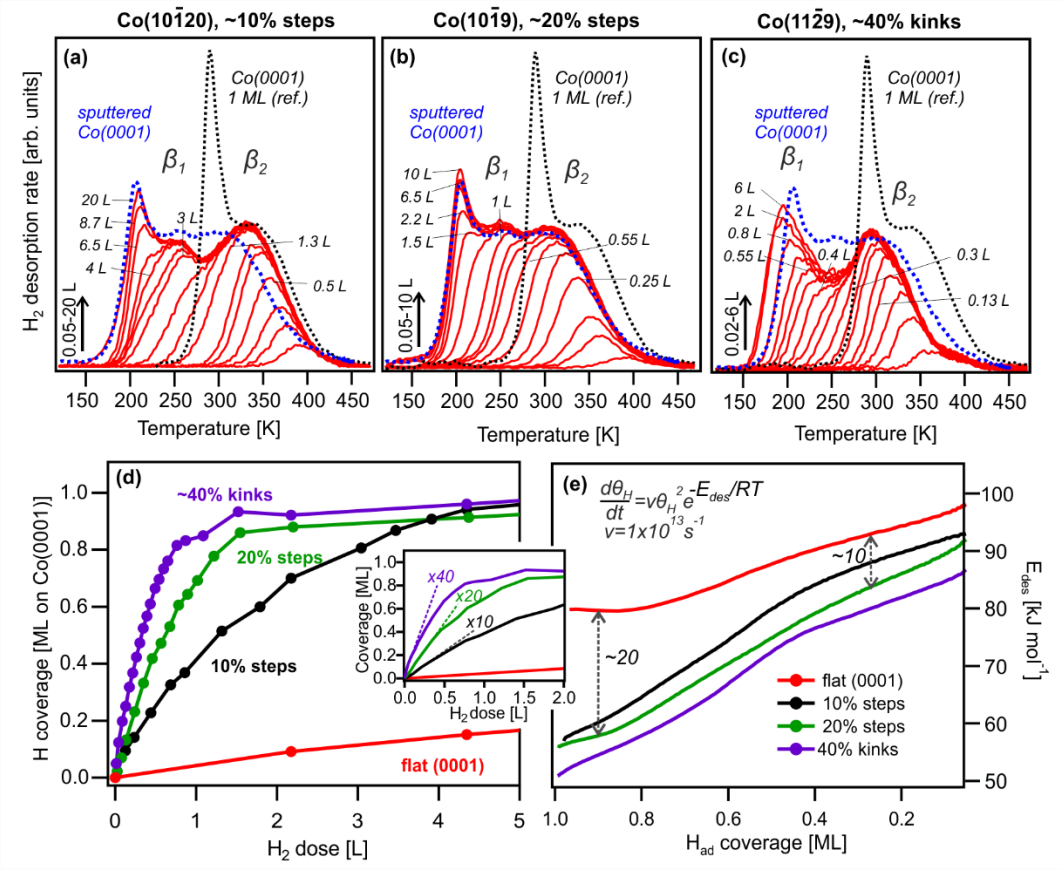

Fig. 7: *(a-c) coverage-dependent H_2 desorption spectra (2 Ks^{-1}) for different stepped and kinked HCP-Co surfaces. The H_2 desorption traces of 1 ML H_{ad} on Co(0001) and on a sputtered-damaged Co(0001) surface (1 keV, 5 min at 350 K) are shown by dashed lines. The corresponding coverage-dose curves are shown in (d). (e) apparent coverage-dependent activation energy for desorption assuming second order desorption and a constant pre-factor of 1×10^{13} s^{-1}.*

Undercoordinated surface atoms present at defects on the close-packed cobalt surface are known to promote dissociative hydrogen adsorption [4,7–9,22]. We here use a collection of regularly stepped and kinked cobalt surfaces to systematically study the influence of undercoordinated sites on dissociative hydrogen adsorption. The LEED patterns for the stepped surfaces [see SI] confirm that the surface structures correspond to the bulk-terminated structures shown in figure 1. Figure 7(a-c) shows the H_2 desorption spectra obtained after dosing H_2 at 100 K on three different vicinal cobalt surfaces. The dose-coverage plots in figure 7(d) show that the sticking probability scales roughly with step density, with a ~10-fold enhancement on the sample with ~10% step site atoms up to a 40-fold enhancement for the sample with ~40% kinked steps. Quantitative evaluation (see experimental section for details) shows that the hydrogen coverage saturates at around 1 ML on all stepped/kinked surfaces, including a sputter-damaged Co(0001) surface.

The Co(10-120) sample has a step density of about 10%, and this relatively small step concentration already has a strong effect on the shape of the hydrogen desorption spectrum. The β_2 peak ($\theta_H \leq 0.5$ ML) shows a small downward shift relative to that on Co(0001) while the downward shift of the β_1 peak ($\theta_H \geq 0.5$ ML) is much larger. Above 0.8 ML an additional sharp desorption peak grows at the low temperature side of the main β_1 peak. Co(10-19) has a step density of around 20%, and this higher concentration causes a further downward shift of the β_2

peak, while the peak shape, area and position of the β_1 peak is similar to that on the 10% stepped sample. The β_1 and β_2 peaks are found at even lower temperature on Co(11-29), which has a step density of around ~40% and contains kink sites. We note that the H_2 desorption spectrum from a sputter-damaged surface [4] is almost identical to that from the sample with 20% steps. STM images in ref. [42] show that sputter-damaged Co(0001) exposes small, close-packed terraces separated by monoatomic step edges. The same structural elements are found on the regularly stepped Co(10-120) and Co(10-19) surfaces and hydrogen desorption therefore proceeds in a similar manner.

Figure 7(e) shows the outcome of a simple analysis of the coverage dependent desorption barrier (E_{des}) for the various surfaces by assuming second order desorption and a constant pre-factor of 1×10^{13} s^{-1}. These traces all show a decrease of the desorption barrier with increasing coverage, with a notable step change around 0.5 ML. This coverage dependence can be traced back to a decrease of the hydrogen adsorption energy, in good agreement with DFT calculations on close-packed surfaces [4,7]. This also agrees well with microcalorimetry experiments on supported cobalt catalysts which show that the differential heat of adsorption gradually decreases from ~100 kJ mol^{-1} at 10% hydrogen coverage to around 60 kJ mol^{-1} for a hydrogen coverage of ~90% [43].

The desorption barriers for the stepped surfaces show a systematic offset relative to the Co(0001) surface. This is related to the hydrogen adsorption barrier and can be understood from the principle of microscopic reversibility: step sites lower the adsorption barrier and due to microscopic reversibility the desorption barrier must be lowered by the same amount. The single activation energy for desorption from a heterogeneous surface as derived in the simplified analysis underlying Fig. 7(e) is an *apparent* desorption barrier which, on a microscopic level, is the sum of desorption from a low barrier route that requires step sites and a high barrier route that occurs on terrace sites. This means that the apparent barrier observed

in the experiment a function of the concentration of step sites together with the barrier difference between the two routes. As a consequence, quantitative description of hydrogen desorption from a stepped surface becomes quite complex as it needs to take many aspects into account: hydrogen desorption requires recombination of *two* hydrogen atom that are not necessarily equivalent as they can occupy either a step or a terrace site. Step sites moreover expose a number of possible sites with different adsorption energies so that a large number of different reaction paths are possible [4,33]. In addition to this, both the adsorption energy and the adsorption barrier vary with hydrogen coverage and finally, entropic factors may affect the desorption kinetics as well. Such a detailed analysis [44,45] is beyond the scope of the present work and we here use a simple model to qualitatively explore how desorption from stepped surface can give rise to only a single desorption peak with a peak temperature that shifts *gradually* with step concentration.

The first simplification made is that the adsorption energies on steps and terraces are assumed to be equal and hydrogen diffusion is fast so that there are no concentration differences between step and terrace sites. The adsorption energy and desorption barrier are both assumed to be independent of coverage, the pre-exponential factor is assumed to be the same for both desorption pathways, and for the mechanism we assume that only one step site is required for the step-assisted desorption route. The net desorption rate then becomes: $\theta_H/dt = n_s \cdot k_s \cdot \theta_H^2 + (1-n_s) \cdot k_t \cdot \theta_H^2$, where n_s is the step concentration and k_s and k_t are the desorption rate constants at steps and terraces, respectively. The difference between the two rate constants is equal to the barrier for dissociative adsorption (E_a), so that $k_s = k_t/\exp(-E_a/RT)$. Several theoretical studies [4,32,33] predict an adsorption barrier of around 8 kJ mol^{-1} on Co(0001) which, at 320 K (the peak maximum of the β_2 peak), translates to a ~20 times higher rate constant for desorption at step sites. Substituting k_s by $20 \cdot k_t$ produces $d\theta_H/dt = (19n_s+1) \cdot k_t \cdot \theta_H^2$, a simple rate expression which shows that the *apparent* rate constant, $(19n_s+1) \cdot k_t$, depends linearly on the concentration of

step sites. This then rationalizes the gradual shift of the desorption peak temperature with step density.

The preceding discussion shows that the lower desorption temperature on vicinal close-packed surfaces is caused by differences in desorption kinetics rather than by adsorption energy differences [44,45]: the phenomenon is in essence caused by the small barrier associated with hydrogen dissociation on the close-packed cobalt surface. Defects do not affect the hydrogen adsorption energy but lower the barrier for dissociative adsorption. As the desorption barrier is lowered by the same amount the presence of defects leads to a lower hydrogen desorption temperature.

Site-dependent heat of adsorption: HCP and FCC surfaces

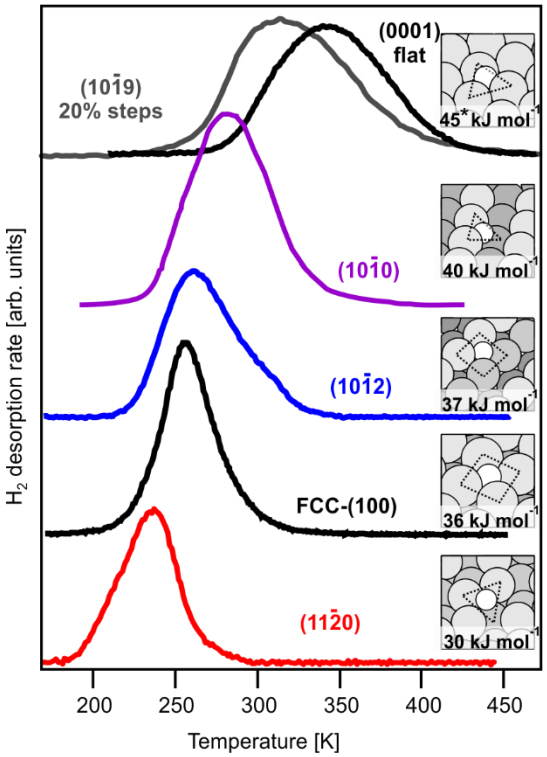

Fig. 8: *A comparison of the H_2 desorption spectrum for ~0.5 ML H_{ad} on various Co surfaces. The spectrum for Co(10-10) was adapted from ref. [3] and those for Co(11-20) and Co(10-12) were adapted from ref. [7]. The insets show the most stable adsorption site predicted by DFT [4,7] together with the adsorption energy (per mol H_{ad}) in the low coverage limit derived*

*from the desorption spectra by assuming a pre-factor of 1×10^{13} s^{-1}. A barrier for adsorption of ~8 kJ per mol H_2 was assumed to calculate the adsorption energy from the barrier for desorption in the case of Co(0001), as discussed in the text. It is marked by * to highlight that it is a special case.*

Fischer-Tropsch synthesis is performed at 475-500 K and in presence of several bars of H_2. The rates of hydrogen adsorption and desorption under these conditions are many orders of magnitude higher than the net hydrogen consumption and the hydrogen coverage is quasi-equilibrated with the gas phase [6]. At first glance one may expect that the higher sticking probability on a defect-rich surface would translate to a higher hydrogen coverage, but this is not the case for a system in equilibrium. The lowering of the adsorption barrier due to the presence of defects is *exactly* balanced by an equal lowering of the desorption barrier so that the equilibrium coverage stays the same. The equilibrium constant, in other words, depends only on the hydrogen adsorption energy even though the adsorption and desorption rates in the dynamic equilibrium are *both* much higher on a defect-containing surface.

This makes the hydrogen adsorption energy the most relevant parameter for applied catalysis as it determines the equilibrium constant for hydrogen adsorption. Information about the structure-dependent adsorption energy can be obtained from a comparison of the H_2 desorption spectra for various cobalt surfaces, provided that the influence of an adsorption barrier is properly accounted for. Hydrogen adsorbs with a high initial sticking probability on all Co surfaces except Co(0001), an indication that adsorption is typically not activated and the adsorption energy can in these cases be taken as equal to the desorption barrier [33]. Barrierless adsorption was proven explicitly for FCC-Co(100) in the preceding sections, and for Co(10-10) the insensitivity of hydrogen adsorption to surface temperature reported by Ernst et al. [3] provides proof for barrierless adsorption on this surface as well. Figure 8 compares the H_2

desorption spectrum from around 0.5 ML H_{ad} on a number of cobalt surfaces, which were in part published previously [3,7]. We note that the spectrum for Co(10-10) was obtained from ref. [3] where a heating rate of 20.5 Ks^{-1} was used. It was adapted using a second order Redhead equation to adjust the temperature scale to match the 2 Ks^{-1} heating rate used for the other data.

The adsorption energy per mol H_{ad} was calculated for each surface by assuming second order desorption and a pre-factor of 1×10^{13} s^{-1}. The value in the low coverage limit (θ_H<0.05 ML) is provided in the figure along with the most stable adsorption site, the latter being derived from DFT calculations in refs. [4,7]. The adsorption energy was assumed to be equal to the desorption barrier for all surfaces except Co(0001), where an ~8 kJ mol^{-1} barrier for H_2 dissociation [4,32,33] was taken into account in the reported value. The barrier for H_2 desorption on Co(10-19) is 90 kJ mol^{-1}, identical to that on the sputtered surface and identical to the value for Co(0001) after subtraction of an 8 kJ mol^{-1} adsorption barrier. It is therefore considered as the most representative for hydrogen adsorption on close-packed terraces and it is therefore included in Fig. 8.

The adsorption energy shows a significant variation with surface structure, where the highest value of around 45 kJ mol^{-1} is found for threefold hollow sites on a close-packed terrace. The adsorption energy on the threefold sites exposed by the more open Co(10-10) is around 40 kJ mol^{-1}, and on the fourfold hollow sites on Co(10-12) and FCC-Co(100) an even lower value of 36 kJ mol^{-1} is found. The lowest value of 30 kJ mol^{-1} corresponds to hydrogen adsorbed in a threefold hollow site on the very open Co(11-20) surface. At 500 K, these differences in adsorption energy translate to a 2-3 order of magnitude difference in the equilibrium constant. As a consequence, the hydrogen concentration under reaction conditions may vary significantly for the different facets of the same catalyst particle. Moreover, the generally weaker adsorption on HCP surfaces would translate to a lower hydrogen equilibrium coverage on HCP-Co particles.

These adsorption energies correspond to the low coverage limit where lateral interactions are absent. Such interactions cause broadening of the desorption peaks below 0.5 ML, and a step change of the adsorption energy around 0.5 ML causes the appearance of an additional low temperature desorption peak for all surfaces considered here with the exception of FCC-Co(100). Such high coverages are less relevant for applied catalysis where the steady state hydrogen coverage is well below 0.5 ML [46,47], but they are relevant for hydrogen chemisorption studies used in cobalt catalyst characterization [43,48]. The hydrogen coverage under reaction conditions is not very high as the active surface during FTS is occupied by other adsorbates, CO being the most abundant [46,49]. CO competes with hydrogen for adsorption sites and may also affect both the hydrogen adsorption kinetics [41] and the hydrogen adsorption energy [6]. Further studies are therefore needed to investigate how the presence of adsorbed CO affects hydrogen adsorption (and vice versa) on flat and stepped surfaces.

Summary and conclusions

The structure-dependent adsorption and desorption of hydrogen on single crystal cobalt surfaces was studied on Co(0001), a thin film of FCC-Co(100) on a copper substrate and three vicinal Co surfaces using temperature programmed desorption and low energy electron diffraction. The initial sticking probability on Co(0001) surface at 100 K is very low but increases with surface temperature. This shows that dissociative hydrogen adsorption is activated on this close-packed cobalt surface, resulting in a low dissociative sticking probability at low surface temperature. This kinetic limitation also makes it difficult to reach a hydrogen coverage above 0.5 ML in UHV experiments. A hot tungsten filament (~1600 K) placed close to the sample surface creates ‘hot’ hydrogen molecules as well as hydrogen atoms that can overcome the dissociation barrier. The combined contributions of both species causes a sixfold increase of the initial dissociative sticking probability at low surface temperature. In addition to this, a hydrogen coverages beyond 0.5 ML can be obtained in this way. Hydrogen in excess

of 0.5 ML desorbs in a separate, low temperature desorption peak. Electron diffraction shows that adsorbate islands with a (2×2)-2H honeycomb structure form between 0.3-0.8 ML, a wide coverage regime that indicates a special stability of this structure. Adsorbed hydrogen in excess of 1 ML is most likely located in subsurface sites, a metastable state that is brought about by reactive hydrogen atoms that are present as a minority species in the hot gas.

Hydrogen adsorption on FCC-Co(100) was studied using a thick (>7 ML) Co film deposited onto a Cu(100) substrate. The initial sticking probability on FCC-Co(100) is around 20 times higher than on the close-packed surface (at 100 K). It is independent of surface temperature, which shows that dissociative hydrogen adsorption is not activated on FCC-Co(100). Hydrogen reaches a saturation coverage of 1 ML and desorption spectra show a single, narrow second order desorption peak for all coverages. Desorption occurs at significantly lower temperatures than from Co(0001), with an estimated barrier for desorption of around 70 kJ mol^{-1} (assuming $\nu=1\times10^{13}$) which is practically independent of the hydrogen coverage. This is quite different for Co(0001), for which the desorption barrier of ~98 kJ mol^{-1} found in the low coverage limit decreases significantly with coverage.

Steps and kinks on the close-packed surface provide a low energy pathway for both dissociative adsorption and recombinative desorption. This results in a dissociative sticking probability that scales with step density as well as a gradual downward shift of the desorption peak with increasing step density. In applied catalysis hydrogen adsorption-desorption is quasi-equilibrated with an equilibrium constant that is determined by the hydrogen adsorption energy. Analysis of the desorption spectra for the various HCP and FCC surfaces shows that hydrogen atoms adsorb most strongly on threefold hollow sites on close-packed terraces while adsorption on the more open FCC-(100) and various HCP surfaces is significantly weaker. The energy differences of 10-15 kJ mol^{-1} (per H_{ads}) translate to an equilibrium constant that is 2-3 orders of magnitude smaller on the more open surfaces. This can have a significant effect on the

equilibrium hydrogen coverage of the different facets of a single particle, and the fact that the adsorption energy is typically lower on surfaces that are present for HCP cobalt nanoparticles would translate to a comparatively lower equilibrium coverage on HCP cobalt.

Acknowledgements

This work has been carried out as part of the SynCat@DIFFER program between the Dutch institute for fundamental energy research (DIFFER), Eindhoven University of Technology (TU/e) and Syngaschem BV and is funded jointly by the Netherlands Organization for Scientific Research (NWO) and Syngaschem BV under project number 731.016.301. Dr. L.B.F. Juurlink (Leiden University) is acknowledged for helpful discussions about the adsorption experiments using a hot filament and the H_2/D_2 exchange reaction. Dr. Pieter van Helden (Sasol) is acknowledged for helpful discussions about the DFT simulations. Syngaschem BV gratefully acknowledges substantial funding from Synfuels China Technology Co. Ltd.

References

(1) Van de Loosdrecht, J.; Botes, F. G.; Ciobica, I. M.; Ferreira, A.; Gibson, P.; Moodley, D. J.; Saib, A. M.; Visagie, J. L.; Weststrate, C. J.; Niemantsverdriet, J. W. Fischer-Tropsch Synthesis: Catalysts and Chemistry. In *Comprehensive Inorganic Chemistry II (Second Edition): From Elements to Applications*; Elsevier Ltd., 2013; Vol. 7, pp 525–557. https://doi.org/10.1016/B978-0-08-097774-4.00729-4.

(2) Sapountzi, F. M.; Gracia, J. M.; Weststrate, C. J.; Fredriksson, H. O. A.; Niemantsverdriet, J. W. Electrocatalysts for the Generation of Hydrogen, Oxygen and Synthesis Gas. *Prog. Energy Combust. Sci.* **2017**, *58*, 1–35. https://doi.org/https://doi.org/10.1016/j.pecs.2016.09.001.

(3) Ernst, K.-H.; Schwarz, E.; Christmann, K. The Interaction of Hydrogen with a

Cobalt(10$\bar{1}$0) Surface. *J. Chem. Phys.* **1994**, *101* (6), 5388. https://doi.org/10.1063/1.467392.

(4) van Helden, P.; van den Berg, J.-A.; Weststrate, C. J. Hydrogen Adsorption on Co Surfaces: A Density Functional Theory and Temperature Programmed Desorption Study. *ACS Catal.* **2012**, *2* (6), 1097–1107. https://doi.org/10.1021/cs2006586.

(5) Huesges, Z.; Christmann, K. Interaction of Hydrogen with a Cobalt(0001) Surface. *Zeitschrift fur Phys. Chemie* **2013**, *227* (6–7), 881–899. https://doi.org/10.1524/zpch.2013.0381.

(6) Weststrate, C. J.; Niemantsverdriet, J. W. Understanding FTS Selectivity: The Crucial Role of Surface Hydrogen. *Faraday Discuss.* **2016**, *197*, 101–116. https://doi.org/10.1039/C6FD00191B.

(7) Weststrate, C. J.; Mahmoodinia, M.; Farstad, M. H.; Svenum, I. H.; Strømsheim, M. D.; Niemantsverdriet, J. W.; Venvik, H. J. Interaction of Hydrogen with Flat (0001) and Corrugated (11–20) and (10–12) Cobalt Surfaces: Insights from Experiment and Theory. *Catal. Today* **2020**, *342*, 124–130. https://doi.org/10.1016/j.cattod.2019.04.002.

(8) Lewis, E. A.; Le, D.; Murphy, C. J.; Jewell, A. D.; Mattera, M. F. G.; Liriano, M. L.; Rahman, T. S.; Sykes, E. C. H. Dissociative Hydrogen Adsorption on Close-Packed Cobalt Nanoparticle Surfaces. *J. Phys. Chem. C* **2012**, *116*, 25868–25873.

(9) Lewis, E. A.; Marcinkowski, M. D.; Murphy, C. J.; Liriano, M. L.; Sykes, E. C. H. Hydrogen Dissociation, Spillover, and Desorption from Cu-Supported Co Nanoparticles. *J. Phys. Chem. Lett.* **2014**, *5* (19), 3380–3385. https://doi.org/10.1021/jz5016789.

(10) Christmann, K. Interaction of Hydrogen with Solid Surfaces. *Surf. Sci. Rep.* **1988**, *9* (1–3), 1–163. https://doi.org/10.1016/0167-5729(88)90009-X.

(11) Kitakami, O.; Sato, H.; Shimada, Y.; Sato, F.; Tanaka, M. Size Effect on the Crystal Phase of Cobalt Fine Particles. *Phys. Rev. B* **1997**, *56* (21), 13849–13854. https://doi.org/10.1103/PhysRevB.56.13849.

(12) van Helden, P.; Ciobîcă, I. M.; Coetzer, R. L. J. The Size-Dependent Site Composition of FCC Cobalt Nanocrystals. *Catal. Today* **2016**, *261*, 48–59. https://doi.org/10.1016/j.cattod.2015.07.052.

(13) Agrawal, R.; Phatak, P.; Spanu, L. Effect of Phase and Size on Surface Sites in Cobalt Nanoparticles. *Catal. Today* **2018**, *312*, 174–180. https://doi.org/https://doi.org/10.1016/j.cattod.2018.03.064.

(14) van Etten, M. P. C.; Zijlstra, B.; Hensen, E. J. M.; Filot, I. A. W. Enumerating Active Sites on Metal Nanoparticles: Understanding the Size Dependence of Cobalt Particles for CO Dissociation. *ACS Catal.* **2021**, 8484–8492. https://doi.org/10.1021/acscatal.1c00651.

(15) van der Niet, M. J. T. C.; den Dunnen, A.; Juurlink, L. B. F.; Koper, M. T. M. The Influence of Step Geometry on the Desorption Characteristics of O 2, D2, and H2O from Stepped Pt Surfaces. *J. Chem. Phys.* **2010**, *132* (17). https://doi.org/10.1063/1.3407434.

(16) van Lent, R.; Auras, S. V.; Cao, K.; Walsh, A. J.; Gleeson, M. A.; Juurlink, L. B. F. Site-Specific Reactivity of Molecules with Surface Defects—the Case of H2 Dissociation on Pt. *Science* **2019**, *363* (6423), 155–157. https://doi.org/DOI: 10.1126/science.aau6716.

(17) Liu, J. X.; Su, H. Y.; Sun, D. P.; Zhang, B. Y.; Li, W. X. Crystallographic Dependence of CO Activation on Cobalt Catalysts: HCP versus FCC. *J. Am. Chem. Soc.* **2013**, *135* (44), 16284–16287. https://doi.org/10.1021/ja408521w.

(18) Falo, F.; Cano, I.; Salmeron, M. CO Chemisorption on Two-Dimensional Cobalt Clusters: A Surface Science Approach to Cluster Chemistry. *Surf. Sci.* **1984**, *143* (1), 303–313. https://doi.org/10.1016/0039-6028(84)90426-6.

(19) Clarke, A.; Jennings, G. .; Willis, R. F. .; Rous, P. J. .; Pendry, J. B. A LEED Determination of the Structrue of Cobalt Overlayers Grown on a Single Crystal Cu(001) Substrate. *Surf. Sci.* **1987**, *187*, 327–338.

(20) Kwak, G.; Woo, M. H.; Kang, S. C.; Park, H. G.; Lee, Y. J.; Jun, K. W.; Ha, K. S. In Situ Monitoring during the Transition of Cobalt Carbide to Metal State and Its Application as Fischer-Tropsch Catalyst in Slurry Phase. *J. Catal.* **2013**, *307*, 27–36. https://doi.org/10.1016/j.jcat.2013.06.029.

(21) Kwak, G.; Kim, D. E.; Kim, Y. T.; Park, H. G.; Kang, S. C.; Ha, K. S.; Jun, K. W.; Lee, Y. J. Enhanced Catalytic Activity of Cobalt Catalysts for Fischer-Tropsch Synthesis: Via Carburization and Hydrogenation and Its Application to Regeneration. *Catal. Sci. Technol.* **2016**, *6* (12), 4594–4600. https://doi.org/10.1039/c5cy01399b.

(22) Chen, Q.; Svenum, I.-H.; Qi, Y.; Gavrilovic, L.; Chen, D.; Holmen, A.; Blekkan, E. A. Potassium Adsorption Behavior on Hcp Cobalt as Model Systems for the Fischer-Tropsch Synthesis: A Density Functional Theory Study. *Phys. Chem. Chem. Phys.* **2017**, *19* (19), 12246–12254. https://doi.org/10.1039/C7CP00620A.

(23) Rendulic, K. D.; Winkler, A.; Steinrück, H. P. The Role of Surface Defects in the Adsorption and Desorption of Hydrogen on Ni(111). *Surf. Sci.* **1987**, *185* (3), 469–478. https://doi.org/10.1016/S0039-6028(87)80171-1.

(24) Habermehl-Ćwirzeń, K. M. E.; Kauraala, K.; Lahtinen, J. Hydrogen on Cobalt: The Effects of Carbon Monoxide and Sulphur Additives on the D2/Co(0001) System. *Phys. Scr.* **2004**, *T108*, 28–32. https://doi.org/10.1238/Physica.Topical.108a00077.

(25) Kizilkaya, A. C.; Niemantsverdriet, J. W.; Weststrate, C. J. Oxygen Adsorption and Water Formation on Co(0001). *J. Phys. Chem. C* **2016**, *120* (9), 4833–4842. https://doi.org/10.1021/acs.jpcc.5b08959.

(26) Weststrate, C. J.; Kizilkaya, A. C.; Rossen, E. T. R. R.; Verhoeven, M. W. G. M.; Ciobîcă, I. M.; Saib, A. M.; Niemantsverdriet, J. W. Atomic and Polymeric Carbon on Co(0001): Surface Reconstruction, Graphene Formation, and Catalyst Poisoning. *J. Phys. Chem. C* **2012**, *116* (21), 11575–11583. https://doi.org/10.1021/jp301706q.

(27) Weststrate, C. J.; van Helden, P.; van de Loosdrecht, J.; Niemantsverdriet, J. W. Elementary Steps in Fischer–Tropsch Synthesis: CO Bond Scission, CO Oxidation and Surface Carbiding on Co(0001). *Surf. Sci.* **2016**, *648*, 60–66. https://doi.org/10.1016/j.susc.2015.10.050.

(28) Allmers, T.; Donath, M. Controlling Cu Diffusion in Co Films Grown on Cu(001). *Surf. Sci.* **2011**, *605* (21–22), 1875–1880. https://doi.org/10.1016/j.susc.2011.05.012.

(29) Klinke, D.; Broadbelt, L. A Theoretical Study of Hydrogen Chemisorption on Ni (111) and Co (0001) Surfaces. *Surf. Sci.* **1999**, *429*, 169–177.

(30) Strømsheim, M. D.; Svenum, I. H.; Farstad, M. H.; Weststrate, C. J. K. J.; Borg, A.; Venvik, H. J. CO-Induced Surface Reconstruction of the Co(11-20) Surface - A Combined Theoretical and Experimental Investigation. *J. Phys. Chem. C* **2020**, *124* (52), 28488–28499. https://doi.org/10.1021/acs.jpcc.0c07852.

(31) Johnson, A. D.; Maynard, K. J.; Daley, S. P.; Yang, Q. Y.; Ceyer, S. T. Hydrogen

Embedded in Ni: Production by Incident Atomic Hydrogen and Detection by High-Resolution Electron Energy Loss. *Phys. Rev. Lett.* **1991**, *67* (7), 927–930. https://doi.org/10.1103/PhysRevLett.67.927.

(32) Jiang, B.; Hu, X.; Lin, S.; Xie, D.; Guo, H. Six-Dimensional Quantum Dynamics of Dissociative Chemisorption of H2 on Co(0001) on an Accurate Global Potential Energy Surface. *Phys. Chem. Chem. Phys.* **2015**, *17*, 23346–23355. https://doi.org/10.1039/c5cp03324a.

(33) Chen, Q.; Svenum, I.; Gavrilovic, L.; Chen, D.; Blekkan, E. A. Effect of Trace Potassium on Hydrogen Adsorption and Dissociation on Hcp Cobalt : A Density Functional Theory Study. *Surf. Sci.* **2019**, *681*, 24–31. https://doi.org/10.1016/j.susc.2018.11.001.

(34) Langmuir, I. The Dissociation of Hydrogen into Atoms [Part II] Calculation of the Degree of Dissociation and the Heat of Formation. *J. Am. Chem. Soc.* **1915**, *37* (3), 417–458. https://doi.org/10.1021/ja02168a002.

(35) Hickmott, T. W. Interaction of Hydrogen with Tungsten. *J. Chem. Phys.* **1960**, *32* (3), 810–823. https://doi.org/10.1063/1.1730802.

(36) Kaminsky, M. Inelastic Collisions of Atoms and Molecules with Metal Surfaces: The Accommodation Coefficient BT - Atomic and Ionic Impact Phenomena on Metal Surfaces; Kaminsky, M., Ed.; Springer Berlin Heidelberg: Berlin, Heidelberg, 1965; pp 56–95. https://doi.org/10.1007/978-3-642-46025-8_6.

(37) Polanyi, J. C. Some Concepts in Reaction Dynamics. *Science.* **1987**, *236*, 680–690.

(38) Domany, E.; Schick, M.; Walker, J. S. Proposed Structure of Hydrogen on Ni(111). *Solid State Commun.* **1979**, *30*, 331–332.

(39) Ciufo, R. A.; Han, S.; Floto, M. E.; Eichler, J. E.; Henkelman, G.; Mullins, C. B. Hydrogen Desorption from the Surface and Subsurface of Cobalt. *Phys. Chem. Chem. Phys.* **2020**, *22* (27), 15281–15287. https://doi.org/10.1039/D0CP02410D.

(40) Chorkendorff, I.; Rasmussen, P. B. Reconstruction of Cu(100) by Adsorption of Atomic Hydrogen. *Surf. Sci.* **1991**, *248* (1–2), 35–44. https://doi.org/10.1016/0039-6028(91)90059-2.

(41) Johansson, M.; Lytken, O.; Chorkendorff, I. The Sticking Probability for H2 in Presence of CO on Some Transition Metals at a Hydrogen Pressure of 1 Bar. *Surf. Sci.* **2008**, *602* (10), 1863–1870. https://doi.org/10.1016/j.susc.2008.03.025.

(42) Böller, B.; Durner, K. M.; Wintterlin, J. The Active Sites of a Working Fischer–Tropsch Catalyst Revealed by Operando Scanning Tunnelling Microscopy. *Nat. Catal.* **2019**. https://doi.org/10.1038/s41929-019-0360-1.

(43) Patanou, E.; Tveten, E. Z.; Chen, D.; Holmen, A.; Blekkan, E. A. Microcalorimetric Studies of H2 and CO on Co/γ-Al2O3 Catalysts for Fischer–Tropsch Synthesis. *Catal. Today* **2013**, *214*, 19–24. https://doi.org/https://doi.org/10.1016/j.cattod.2012.12.006.

(44) Poelsema, B.; Lenz, K.; Comsa, G. The Dissociative Adsorption of Hydrogen on Defect-'free' Pt(111). *J. Phys. Condens. Matter* **2010**, *22* (30). https://doi.org/10.1088/0953-8984/22/30/304006.

(45) Poelsema, B.; Lenz, K.; Comsa, G. The Dissociative Adsorption of Hydrogen on Pt(111): Actuation and Acceleration by Atomic Defects. *J. Chem. Phys.* **2011**, *134* (7). https://doi.org/10.1063/1.3530286.

(46) Den Breejen, J. P.; Radstake, P. B.; Bezemer, G. L.; Bitter, J. H.; Frøseth, V.; A. Holmen; de Jong, K. P. On the Origin of the Cobalt Particle Size Effects in Fischer-

Tropsch Catalysis. *J. Am. Chem. Soc.* **2009**, *131* (20), 7197–7203. https://doi.org/10.1021/ja901006x.

(47) van Helden, P.; van den Berg, J. A.; Petersen, M. A.; Janse van Rensburg, W.; Ciobica, I. M.; van de Loosdrecht, J. Computational Investigation of the Kinetics and Mechanism of the Initial Steps of the Fischer–Tropsch Synthesis on Cobalt. *Faraday Discuss.* **2017**, *197*, 117–151.

(48) Reuel, R. C.; Bartholomew, C. H. The Stoichiometries of H2 and CO Adsorptions on Cobalt: Effects of Support and Preparation. *J. Catal.* **1984**, *85* (1), 63–77. https://doi.org/10.1016/0021-9517(84)90110-6.

(49) Schweicher, J.; Bundhoo, A.; Kruse, N. Hydrocarbon Chain Lengthening in Catalytic CO Hydrogenation: Evidence for a CO-Insertion Mechanism. *J. Am. Chem. Soc.* **2012**, *134* (39), 16135–16138. https://doi.org/10.1021/ja3068484.